Published in final edited form as:
Nat Synth. 2023 August ; 2(8): 740–748. doi:10.1038/s44160-023-00286-7.

A general method for metallocluster site-differentiation

Trever M. Bostelaar,
Alexandra C. Brown,
Arun Sridharan,
Daniel L. M. Suess
Department of Chemistry, Massachusetts Institute of Technology, Cambridge, MA, USA

Abstract

The deployment of metalloclusters in applications such as catalysis and materials synthesis requires robust methods for site-differentiation: the conversion of clusters with symmetric ligand spheres to those with unsymmetrical ligand spheres. However, imparting precise patterns of site-differentiation is challenging because, compared with mononuclear complexes, the ligands bound to clusters exert limited spatial and electronic influence on one another. Here, we report a method that employs sterically encumbering ligands to bind to only a subset of a cluster's coordination sites. Specifically, we show that homoleptic, phosphine-ligated Fe–S clusters undergo ligand substitution with *N*-heterocyclic carbenes (NHCs) to give heteroleptic clusters in which the resultant clusters' site-differentiation patterns are encoded by the steric profile of the incoming NHC. This method affords access to every site-differentiation pattern for cuboidal [Fe_4S_4] clusters and can be extended to other cluster types, particularly in the stereoselective synthesis of site-differentiated Chevrel-type [Fe_6S_8] clusters.

Graphical Abstract

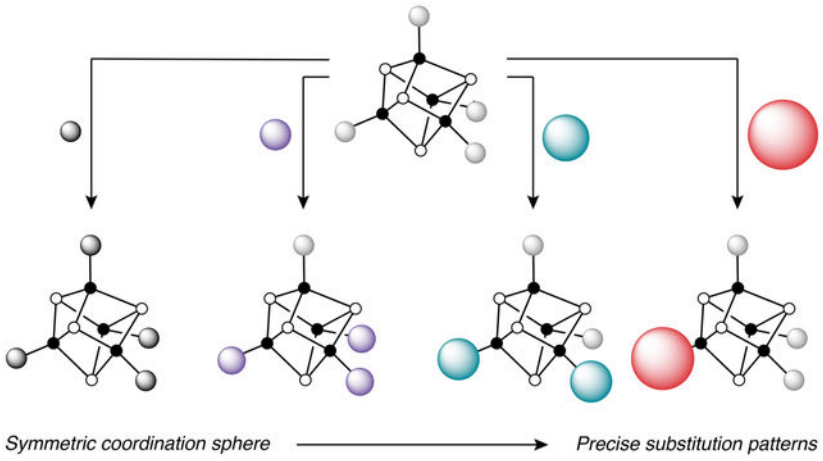

Author Contributions Statement
T.A.B., A.C.B., and A.S. performed the experiments. All authors analyzed the data and contributed to the manuscript writing.

Competing Interests Statement
The authors declare no competing financial interest.

Introduction

Compared with single metal centers, metalloclusters offer additional compositional tunability, novel electronic structures, and unique modes of reactivity with substrates (*e.g.*, via metal–metal cooperativity or multi-site reactivity).[1–8] For these and other reasons, atomically precise metalloclusters are finding increasing use in various contexts including bioinorganic chemistry,[9–12] materials synthesis,[13–20] and catalysis.[21–23] Synthetic methodology is foundational to these efforts, underlying both cluster assembly and subsequent coordination chemistry. Regarding the latter, it is critical to be able to control a cluster's coordination sphere—the identity and stereochemical arrangement of its ligands—ideally with similar precision as has been achieved for mononuclear complexes.[24] A major obstacle is that, unlike for mononuclear complexes, the ligands in clusters are bound to different metal centers, which are typically separated by at least several angstroms. As a result, the spatial and electronic interactions between a ligand and the rest of the cluster (the metal centers as well as the other ligands) are weak. This fundamental difference between the coordination chemistry of clusters and that of mononuclear complexes has several consequences, and we focus herein on how it affects one of the simplest elementary reactions: ligand substitution, particularly in the conversion of highly symmetric, undifferentiated clusters (in which the same ligands bind to chemically equivalent metal centers) to site-differentiated clusters (in which a particular ligand binds to only a subset of the metal centers, thereby imparting chemical inequivalence).

Site-differentiated clusters have broad utility, including as structural and functional models of biological metalloclusters[25–33] and as building blocks in materials synthesis.[20,34–36] However, imparting site-differentiation remains a substantial synthetic challenge, as illustrated in Fig. 1 for a generic cluster in which the metal ions are arranged in a tetrahedron (*e.g.*, in a cuboidal [Fe_4S_4] cluster). Typically, ligand substitution reactions at such clusters generate mixtures of unsubstituted, monosubstituted, disubstituted, trisubstituted, and tetrasubstituted products (n = 0–4, respectively, for n substitution events; Fig. 1A), where the ratio of the products depends primarily on the stoichiometry of the incoming ligand (x; Fig. 1B). Such mixtures are generated because, to a first approximation, ligand substitution at one site will minimally impact the kinetics or thermodynamics of ligand substitution at another, resulting in mixtures of partially substituted clusters.[37] The stochastic nature of ligand substitution has been a long-standing challenge in metallocluster coordination chemistry,[37–40] and although there are many examples of site-differentiated clusters, their preparation often relies on the unique solubility properties of partially substituted clusters,[20,41–43] on chromatographic separation of clusters with different site-differentiation patterns,[39,44] or on the use of carefully designed, chelating ligands.[25,26,28–30,33] As such, there remains a need for general, robust methods for the selective synthesis of site-differentiated clusters.

We herein report such a method that uses the steric properties of monodentate ligands to impart site-differentiation. In this approach (Fig. 1C), the size of the incoming ligand dictates the maximum number of substitution events that can occur (m) whereby over-substitution is prevented because additional ligands cannot fit around the cluster. Thus, a particular site-differentiation pattern can be obtained simply by adding an excess of a

ligand ($x \geq m$) that has the appropriate steric properties. Support for this approach includes examples of metallocluster self-assembly reactions in which the product is dictated by the steric properties of the ligand,[45–47] as well as reports of partial ligand substitution at polycarbonylated Fe clusters using bulky isocyanides or phosphines (giving rise to products with asymmetric substitution patterns).[48,49] In the current work, we develop this method using cuboidal [Fe_4S_4] clusters, which serve as models for active sites of Fe–S proteins,[3,12,50–52] and we show that it can be extended to Chevrel-type [Fe_6S_8] clusters, which have garnered interest as building blocks in extended solids.[53] Experiments with the Chevrel-type clusters demonstrate that, in addition to dictating the number of substitution events, the incoming ligand's steric profile can control the cluster's stereochemistry, enabling site-differentiation with high diastereoselectivity.

Results and Discussion

We initiated our study by investigating substitution reactions of cuboidal [Fe_4S_4] clusters with *N*-heterocyclic carbenes (NHCs), which form relatively strong Fe–C bonds[54] and have highly tunable steric properties.[55] Moreover, previous work from our laboratory has established that installing bulky NHCs onto pre-site-differentiated clusters enhances the stability of the clusters with respect to disproportionation to undifferentiated clusters (a common side-reaction in metallocluster chemistry).[32] In the present work, we utilize NHCs to transform *undifferentiated* clusters into clusters with precise patterns of site-differentiation.

We first examined the substitution of the PCy_3 ligands of the undifferentiated cluster [$Fe_4S_4(PCy_3)_4$][BPh_4] (**1**)[46] with a series of *N*-aryl NHCs in which the steric properties of the aryl groups are systematically tuned (Fig. 2). Beginning with the smallest NHC in the series, ITol (1,3-di-*p*-tolylimidazol-2-ylidene), we observed that adding excess ITol (5 equiv) to **1** resulted in complete substitution of the PCy_3 ligands. This was evident from the crude ^{31}P NMR spectrum, which showed the disappearance of the resonance corresponding to **1** at 324 ppm, the generation of free PCy_3 at 10.7 ppm, and no additional resonances corresponding to species with cluster-bound PCy_3 ligands. The identity of the product as [$Fe_4S_4(ITol)_4$][BPh_4] (**2**) was confirmed by single-crystal X-ray diffraction (XRD) analysis (Fig. 2B). Therefore, ITol, like the smaller *N*-alkyl NHC I^iPr^{Me} (I^iPr^{Me} = 1,3-diisopropyl-4,5-dimethylimidazol-2-ylidene) can bind [Fe_4S_4] clusters at all four Fe sites.[32,54]

The analogous reaction with IMes (1,3-dimesitylimidazol-2-ylidene; 5 equiv) yielded a different outcome. In addition to the peak corresponding to free PCy_3, a paramagnetically shifted peak was observed at 289 ppm in the ^{31}P NMR spectrum of the reaction mixture, indicating at least one PCy_3 ligand remained bound to the cluster. Purification and characterization of the product revealed its identity as the trisubstituted cluster [$Fe_4S_4(PCy_3)(IMes)_3$][BPh_4] (**3**). Here, despite the thermodynamic favorability of substituting a phosphine with an NHC,[54,56] complete substitution does not occur because a fourth IMes ligand is too sterically encumbering to bind. The partial substitution of [Fe_4S_4] clusters by bulky ligands has clear parallels in the chemistry of metalloclusters (*vide supra*) and

mononuclear complexes, for example in substitution reactions of phosphines with NHCs in the synthesis of Ru metathesis catalysts.[56,57]

Further increasing the bulkiness of the *ortho* substituents from methyl to isopropyl (IPr; 1,3-bis(2,6-diisopropylphenyl)imidazol-2-ylidene) halts substitution after the second event. Specifically, the maximally substituted product of the reaction of excess IPr (5 equiv) with **1** is the disubstituted cluster $[Fe_4S_4(PCy_3)_2(IPr)_2][BPh_4]$ (**4**) in which two PCy_3 ligands remain bound to the cluster ($\delta(^{31}P)$ = 390 ppm). Efficient conversion of **1** to **4** required refluxing the reaction mixture for 3 h. The relatively slow rate of ligand substitution, particularly for the second substitution event, is evident in reactions monitored by ^{31}P NMR spectroscopy at room temperature (Fig. S4) and contrasts the behavior of the smaller NHCs (ITol and IMes) for which the maximally substituted clusters are obtained within minutes at room temperature. These observations highlight the importance of the size of the *ortho* substituent on the kinetics and the thermodynamics of ligand substitution.

In an initial attempt to generate a monosubstituted cluster of the form $[Fe_4S_4(PCy_3)_3(NHC)][BPh_4]$, we mixed **1** with the bulky NHC IPr* (1,3-bis(2,6-bis(diphenylmethyl)-4-methylphenyl)imidazol-2-ylidene). However, only slow decomposition was observed, with no evidence for ligand substitution; apparently, the *ortho*-diphenylmethyl substituents render IPr* too large to fit onto the cluster. Paring down the steric profile to ITpp (1,3-bis(2,4,6-triphenylphenyl)imidazol-2-ylidene) achieved the desired outcome: the monosubstituted cluster $[Fe_4S_4(PCy_3)_3(ITpp)][BPh_4]$ (**5**; $\delta(^{31}P)$ = 348 ppm). Here, the massive steric profile of ITpp—specifically, perpendicular to the imidazolyl ring—prevents a second substitution event, leaving the other three Fe sites bound to PCy_3 even in the presence of excess ITpp. Performing an analogous reaction with IDpp (1,3-bis(2,6-diphenylphenyl)imidazol-2-ylidene; identical to ITpp but lacking the *para*-phenyl substituents on the Ar group) also yields a monosubstituted cluster, $[Fe_4S_4(PCy_3)_3(IDpp)][BPh_4]$ (**6**; $\delta(^{31}P)$ = 339 ppm; *vide infra*). Thus, the *para*-phenyl substituents on the *N*-aryl groups of ITpp play no role in halting disubstitution, and the observed monosubstitution pattern for both can be attributed to the *ortho*-phenyl groups. Both ITpp and IDpp react slowly with **1** and the reaction conditions that give high conversion (70 °C, THF) also yield some unidentified byproducts. As such, **5** and **6** were not isolated as pure materials, though NMR spectroscopic analysis of both species (Figs. S6 and S7) and single-crystal XRD analysis of **5** (Fig. 2) confirmed their identities.

Notably, in the syntheses of **2**–**6**, under no conditions did we observe further substitution by additional NHC equivalents beyond the maximum shown in Fig. 2. Although we attribute this to thermodynamic reasons (*i.e.*, that additional NHC ligands simply cannot fit around the cluster), we cannot rule out the possibility that additional substitution events are only kinetically disfavored. Regardless, the outcome is the same: precise site-differentiation patterns can be imparted to $[Fe_4S_4]$ clusters by rationally tuning the *N*-aryl substitutions of NHCs.

The solid-state structures of **2**–**5** were established by single-crystal XRD analysis (Fig. 2). The ligand sphere of **2** confers nearly S_4 symmetry to the cluster, whereas the three IMes ligands in **3** form a C_3-like pocket that harbors the cluster core and the PCy_3 ligand,

similarly to other tris-IMes-ligated [Fe_4S_4] clusters.[32,58–63] Cluster **4** is positioned on a crystallographic two-fold rotational axis and its two IPr ligands form a clamshell-like pocket in which the cluster sits. The steric profile of the lone ITpp ligand in **5** is comparatively flat, and as suggested by the space-filling model, no more than one ITpp ligand can fit around the cluster. For **2**–**5**, the Fe–C bond lengths fall in a narrow range (the shortest distance is 2.060(2) Å in **5** and the longest is 2.082(1) Å in **2**) and are in line with those observed for other NHC-ligated [Fe_4S_4] clusters.[32,54,58–63] Similarly, the Fe–P bonds in the series fall between 2.3874(8) Å in **5** and 2.4159(8) Å in **4**, fully within the range of Fe–P distances reported for **1** (2.371(2)–2.428(3) Å).[46] Each NHC-ligated cluster displays a tetragonal compression along four Fe–S bonds as is commonly observed for $[Fe_4S_4]^+$ clusters,[64] and there is no statistically significant difference in the average Fe–S distances of NHC-ligated Fe sites compared to phosphine-ligated Fe sites. The absence of any meaningful differences in Fe–C, Fe–P, and cluster core bond metrics leads us to rule out the possibility that the observed site-differentiation patterns are a result of the bulky NHCs perturbing the cluster core's geometric or electronic structures (though, as expected from previous work,[54] substitution of phosphines by NHCs does make the clusters more electron-rich; see the SI for the cyclic voltammograms of **1**–**4**).

Although the trend observed for the series **2**–**5** is qualitatively sensible—the NHCs with larger aryl groups give rise to a decreased maximum number of ligand substitution events, *m*—we sought a parameter based on the NHC steric profile that would predict *m*. For this purpose, we needed to analyze the substitution chemistry of a larger number of NHCs with a broader range of structural features. This objective was accomplished by preparing a small library of NHCs, titrating each individually into solutions of **1**, and monitoring the reactions by ^{31}P NMR spectroscopy (Fig. 3A). To illustrate, we describe the results for IMes (Fig. 3B). As stated above, the starting cluster **1** gives rise to a peak in the ^{31}P NMR spectrum at 324 ppm that decreases in intensity with added IMes. Intermediates *en route* to the fully substituted cluster **3** emerge first at 311 ppm, then at 233 ppm. These features disappear with ≥3 equiv IMes (at which point only **3** is present at 289 ppm) and can therefore be assigned to the mono- and disubstituted clusters, $[Fe_4S_4(PCy_3)_3(IMes)][BPh_4]$ and $[Fe_4S_4(PCy_3)_2(IMes)_2][BPh_4]$, respectively. Using this procedure, we determined the maximal substitution number for a total of eleven NHCs (Fig. 3A; see SI Fig. S40–S52 for spectra). Of the new clusters generated in these experiments, $[Fe_4S_4(IMesCy)_4][BPh_4]$ (**7**; IMesCy, 1-cyclohexyl-3-mesitylimidazol-2-ylidene) was isolated and structurally characterized (Fig. S54). In short, we found that ITol, ICy (1,3-dicyclohexylimidazol-2-ylidene), and IMesCy fully substitute **1** ($m = 4$); IMes, IDep (1,3-bis(2,6-diethylphenyl)imidazol-2-ylidene), and IMesAd (1-adamantyl-3-mesitylimidazol-2-ylidene) result in trisubstitution ($m = 3$); IPr, SIAnt (1,3-di(anthracene-9-yl)-4,5-dihydroimidazol-2-ylidene), and ITppCy (1-cyclohexyl-3-(2,4,6-triphenylphenyl)imidazol-2-ylidene) substitute twice ($m = 2$); and ITpp and IDpp substitute once ($m = 1$; *vide supra*). The structural diversity of the NHCs that can effect well-defined site-differentiation—those having symmetric or asymmetric *N* substituents, alkyl and/or aryl substituents, and saturated or unsaturated backbone rings—highlights the generality of this approach.

With the *m* values for a wide range of NHCs in hand, we sought to identify a steric parameterization that could predict the experimentally observed substitution chemistry. We found that the solid angle[65] is suitable for this purpose; an alternative metric, the percent buried volume,[66] gives qualitatively similar but somewhat poorer results and is discussed in the SI. The theoretical solid angles, G_T, were computed for each NHC in Fig. 3A using atomic coordinates obtained from geometry optimizations of $FeCl_3$(NHC) model complexes with a fixed Fe–C bond length of 2 Å (see SI for details), and the resulting values were plotted against *m* (Fig. 3C). The calculated G_T values of each NHC correlate well with substitution number: NHCs with $G_T \leq$ *ca.* 36% are observed to substitute up to four times, those within the narrow range of *ca.* 40% $\leq G_T \leq$ *ca.* 41% up to three times, and those with *ca.* 42% $\leq G_T \leq$ *ca.* 46% up to twice. The observation that IPr substitutes twice while IDpp substitutes only once suggests that disubstitution stops at a G_T value between 46–50%.

Although the foregoing analysis demonstrates that G_T correlates strongly with *m*, there is likely no strict cutoff between *m* values because G_T (or any steric parameter) cannot fully capture the spatial considerations that influence these reactions. For example, IDep and SIAnt have nearly identical G_T values (41.2% and 41.5%, respectively), yet SIAnt substitutes twice and IDep substitutes thrice. Additionally, we note that G_T is not well-suited for predicting maximum substitution numbers for NHCs with steric bulk concentrated near the metal center. For example, I*t*Bu (1,3-di-*tert*-butylimidazol-2-ylidene) has a relatively low G_T value of 36.2%, yet, under our reaction conditions, it does not bind **1**, presumably because of the significant steric bulk from the tertiary *N*-alkyl substituents oriented directly towards the metal center (*c.f.* ICy, with a G_T value of 32.0%, which has secondary *N*-alkyl substituents and fully substitutes the cluster). Nonetheless, outside of these exceptions (which are also not accurately predicted by the percent buried volume; see SI), the solid angle is a useful metric for predicting the observed substitution behavior of NHCs at cuboidal $[Fe_4S_4]$ clusters.

As noted in the Introduction, the difficulty in imparting site-differentiation—in particular, the stochastic nature of ligand substitution—is not unique to cuboidal clusters featuring tetrahedral metal cores, and instead applies to virtually any highly symmetric, polyhedral cluster. Of these, octahedral $[M_6E_8L_6]$ Chevrel-type clusters present substantial challenges because ligand substitution reactions can yield reaction mixtures with up to ten possible species, several of which are stereoisomers (Fig. 4A). We hypothesized that, as for the cuboidal $[Fe_4S_4]$ clusters, the distal bulk of NHCs could be leveraged to exert steric control over both the substitution number and the stereochemistry of site-differentiated Chevrel-type clusters (Fig. 4A).

To test this hypothesis, we conducted analogous experiments to those described above, except using $[Fe_6S_8(PEt_3)_6][BF_4]$ (**8**)[67] instead of **1**. We first mixed **8** with an excess (8 equiv) of the relatively small NHC, ICy, which resulted in the precipitation of a black solid identified as $[Fe_6S_8(ICy)_6][BF_4]$ (**9**) in which all six PEt_3 ligands from **8** had been substituted by ICy (Fig. 4B and 4C). Interestingly, a relatively modest increase in the NHC steric profile from ICy to IMes resulted in a dramatically different reaction outcome (Fig. 4B). Specifically, mixing **8** with IMes (4 equiv) yielded *trans*-$[Fe_6S_8(PEt_3)_4(IMes)_2][BF_4]$ (**10**) (Fig. 4B and 4D). Under no conditions have we observed either further substitution

of **10** by IMes or formation of the *cis* isomer of **10**. Thus, **10** is produced without complications from over-substitution and with perfect stereoselectivity. Moreover, the fact that hexasubstitution occurs in the preparation of **9** indicates that IMes (which, like ICy, is a stronger donor than PEt_3)[68,69] would likewise undergo six substitution events if not for its more imposing steric profile; we therefore conclude that the basis for stereoselective disubstitution in **10** is steric rather than electronic in origin. The imposing steric profile of IMes with respect to the $[Fe_6S_8]^+$ cluster is evident by the observation that IMes and PEt_3 bind competitively (necessitating the removal of PEt_3 in the synthesis of **10**; see SI). Notably, a few $[M_6E_8]$ clusters bearing NHC ligands have been reported, and each shows a similar *trans* disposition of the NHC ligands;[70] however, as each was prepared from heteroleptic clusters, the site-differentiation pattern and stereochemistry of the product were likely derived from the starting cluster rather than from the steric profile of the NHC.

Both **9** and **10** crystallize in P1” with two half-molecules in the asymmetric unit to give two crystallographically unique clusters that each lie on an inversion center; **9** was crystallographically characterized with a $[BPh_4]^-$ anion, installed *via* salt metathesis (see SI). In **9**, each of the twelve cyclohexyl methine protons bisect the S–Fe–S angle (Fig. 4C). This arrangement yields a configuration in which the cyclohexyl groups reside over a neighboring imidazolyl ring, giving a cluster with approximate T_h symmetry. For IMes, the *ortho*-methyl groups project over the imidazolyl ring (Fig. 4D), and thus would block such an arrangement and prevent binding of *cis*-IMes ligands. Furthermore, the orientation of the IMes ligands in **10** is rotated ~45° with respect to the ICy ligands in **9**, and this configuration may allow the *ortho*-methyl protons to avoid clashing with the bridging sulfides and/or the equatorial PEt_3 ligands. (Fig. 4D, right).

Conclusion

Using two ubiquitous cluster structures, we showed that simple ligand substitution reactions can convert homoleptic clusters to site-differentiated clusters, whereby the pattern of site-differentiation is dictated by the ligands’ steric properties. For cuboidal $[Fe_4S_4]^+$ clusters, this enabled the selective preparation of site-differentiated clusters *via* rational tuning of the aryl substituents of the incoming NHC ligands. In an extension to octahedral, Chevrel-type clusters, we demonstrated that site-differentiated clusters can be obtained in a similar manner and with high stereoselectivity. We anticipate that this method can be generalized to metalloclusters of nearly any composition and geometry, and that these findings will accelerate the application of metalloclusters in catalysis and materials science.

Methods

General considerations

Unless otherwise noted, all reactions were performed using standard Schlenk techniques or in an LC Technologies inert atmosphere glovebox under an N_2 atmosphere. Glassware was dried in an oven at 160 °C prior to use. Molecular sieves (3 Å) and Celite were activated by heating to 300 °C overnight under vacuum prior to storage under an N_2 atmosphere. *o*-Difluorobenzene (DFB) was distilled from CaH_2, THF was distilled from Na benzophenone, C_6D_6 and CD_3CN were degassed by three freeze-pump-thaw cycles, and other solvents

were degassed by sparging with argon and dried by passing through a column of activated alumina. All solvents were stored under an N_2 atmosphere over 3 Å molecular sieves for at least 12 h prior to use. For synthetic protocols and characterization details see SI.

Titration experiments

Titration experiments were conducted via two procedures depending on the solubility of the *N*-heterocyclic carbene ligand. Each titration point (e.g., 1 equiv, 2 equiv, etc.) was prepared independently from stock solutions, as opposed to sequential addition of NHC to a single sample. That each sample was at equilibrium was established by monitoring the composition by ^{1}H and ^{31}P NMR spectra over a 3-hour time period. All NMR spectra were recorded using identical acquisition parameters, and all titration points for each NHC were collected on the same instrument.

Procedure A: This method was employed for NHCs with good solubility in THF (ICy, IMesCy, IMesAd, IMes, IDep, IPr). In an NMR tube containing a solution of **1** (15.2 mM) in THF, aliquots of an NHC stock solution in THF (164 mM) were added via syringe. For IPr, the reaction was heated to 70 °C for 3 hours.

Procedure B: This method was employed for NHCs with poor solubility in THF (ITol, SIAnt, ITppCy, IDpp, and ITpp). Solid NHC was weighed into small crystallization vials. The solid NHC was suspended in 250 μL THF and, with vigorous stirring, a stock solution of **1** (15.2 mM) in THF was added rapidly via syringe. For IDpp and ITpp, the reactions were heated to 70 °C for 2 hours.

Supplementary Material

Refer to Web version on PubMed Central for supplementary material.

Acknowledgements

The authors thank N. B. Lewis and M. Kumar for assistance with HRMS experiments, as well as P. Müller for assistance with XRD experiments. This work was supported by the National Institute of General Medical Sciences of the National Institutes of Health under award number R01GM136882 (D.L.M.S.) and by seed funding from the American Chemical Society Petroleum Research Fund under award number 60568-DNI3 (D.L.M.S.). A.C.B. acknowledges fellowships from MathWorks, the National Science Foundation (Graduate Research Fellowship no. 1122374), and the Fannie and John Hertz Foundation.

Data availability

All characterization data, computational data, and experimental protocols are provided in the Supplementary Information. Crystallographic data for the structures reported in this Article have been deposited at the Cambridge Crystallographic Data Centre, under deposition numbers CCDC 2214357–2214363. Copies of the data can be obtained free of charge via https://www.ccdc.cam.ac.uk/structures. Coordinates of optimized structures are included as Supplementary Information.

References

(1). Muetterties EL Metal Clusters in Catalysis III.—Clusters as Models for Chemisorption Processes and Heterogeneous Catalysis. Bull. des Sociétés Chim. Belges 1975, 84 (10), 959–986.

(2). Lee SC; Holm RH Nonmolecular Metal Chalcogenide/Halide Solids and Their Molecular Cluster Analogues. Angew. Chemie Int. Ed 1990, 29 (8), 840–856.

(3). Beinert H; Holm RH; Munck E Iron-Sulfur Clusters: Nature's Modular, Multipurpose Structures. Science 1997, 277 (5326), 653–659. [PubMed: 9235882]

(4). Sokolov MN; Fedin VP; Sykes AG Chalcogenide-Containing Metal Clusters. In Comprehensive Coordination Chemistry II; McCleverty JA, Meyer TJ, Wedd AG, Eds.; Elsevier Pergamon, 2003; Vol. 4, p 761.

(5). Degroot MW; Corrigan JF High Nuclearity Clusters: Metal–Chalcogenide Polynuclear Complexes. In Comprehensive Coordination Chemistry II; McCleverty JA, Meyer TJ, Fujita M, Powell AK, Creutz CA, Eds.; Elsevier Pergamon, 2003; Vol. 7, pp 57–123.

(6). Jena P; Sun Q Super Atomic Clusters: Design Rules and Potential for Building Blocks of Materials. Chem. Rev 2018, 118 (11), 5755–5870. [PubMed: 29812916]

(7). Doud EA et al. Superatoms in Materials Science. Nat. Rev. Mater 2020, 5 (5), 371–387.

(8). Cesari C; Shon JH; Zacchini S; Berben LA Metal Carbonyl Clusters of Groups 8–10: Synthesis and Catalysis. Chem. Soc. Rev 2021, 50 (17), 9503–9539. [PubMed: 34259674]

(9). Venkateswara Rao P; Holm RH Synthetic Analogues of the Active Sites of Iron- Sulfur Proteins. Chem. Rev 2004, 104 (2), 527–560. [PubMed: 14871134]

(10). Lee SC; Lo W; Holm RH Developments in the Biomimetic Chemistry of Cubane-Type and Higher Nuclearity Iron--Sulfur Clusters. Chem. Rev 2014, 114 (7), 3579–3600. [PubMed: 24410527]

(11). Rathnayaka SC; Mankad NP Coordination Chemistry of the CuZ Site in Nitrous Oxide Reductase and Its Synthetic Mimics. Coord. Chem. Rev 2021, 429, 213718. [PubMed: 33692589]

(12). Bigness A; Vaddypally S; Zdilla MJ; Mendoza-Cortes JL Ubiquity of Cubanes in Bioinorganic Relevant Compounds. Coord. Chem. Rev 2022, 450, 214168.

(13). Bag S; Trikalitis PN; Chupas PJ; Armatas GS; Kanatzidis MG Porous Semiconducting Gels and Aerogels from Chalcogenide Clusters. Science 2007, 317 (5837), 490–493. [PubMed: 17656718]

(14). Claridge SA; Castleman AW; Khanna SN; Murray CB; Sen A; Weiss PS Cluster-Assembled Materials. ACS Nano 2009, 3 (2), 244–255. [PubMed: 19236057]

(15). Roy X et al. Nanoscale Atoms in Solid-State Chemistry. Science 2013, 341 (6142), 157–160. [PubMed: 23744780]

(16). Tomalia DA; Khanna SNA Systematic Framework and Nanoperiodic Concept for Unifying Nanoscience: Hard/Soft Nanoelements, Superatoms, Meta-Atoms, New Emerging Properties, Periodic Property Patterns, and Predictive Mendeleev-like Nanoperiodic Tables. Chem. Rev 2016, 116 (4), 2705–2774. [PubMed: 26821999]

(17). Horwitz NE et al. Redox-Active 1D Coordination Polymers of Iron--Sulfur Clusters. J. Am. Chem. Soc 2019, 141 (9), 3940–3951. [PubMed: 30715871]

(18). Zhang J; Bu X; Feng P; Wu T Metal Chalcogenide Supertetrahedral Clusters: Synthetic Control over Assembly, Dispersibility, and Their Functional Applications. Acc. Chem. Res 2020, 53 (10), 2261–2272. [PubMed: 32877164]

(19). Gillen JH et al. Synthesis and Disassembly of an Organometallic Polymer Comprising Redox-Active Co_4S_4 Clusters and Janus Biscarbene Linkers. Chem. Commun 2022, 58 (31), 4885–4888.

(20). Bartholomew AK et al. Superatom Regiochemistry Dictates the Assembly and Surface Reactivity of a Two-Dimensional Material. J. Am. Chem. Soc 2022, 144 (3), 1119–1124. [PubMed: 35020382]

(21). Kephart JA; Mitchell BS; Kaminsky W; Velian A Multi-Active Site Dynamics on a Molecular Cr/Co/Se Cluster Catalyst. J. Am. Chem. Soc 2022, 144 (21), 9206–9211. [PubMed: 35593888]

(22). McCool NS; Robinson DM; Sheats JE; Dismukes GC A Co_4O_4 Cubane Water Oxidation Catalyst Inspired by Photosynthesis. J. Am. Chem. Soc 2011, 133 (30), 11446–11449. [PubMed: 21739983]

(23). Li G; Jin R Atomically Precise Gold Nanoclusters as New Model Catalysts. Acc. Chem. Res 2013, 46 (8), 1749–1758. [PubMed: 23534692]

(24). Pombeiro AJL; Kukushkin VY Ligand Reactivity: General Introduction. In Comprehensive Coordination Chemistry II; McCleverty JA, Meyer TJ, Lever ABP, Eds.; Elsevier Pergamon, 2003; Vol. 1, pp 585–594.

(25). Stack TDP; Holm RH Subsite-Specific Functionalization of the $[4Fe\text{-}4S]^{2+}$ Analog of Iron-Sulfur Protein Clusters. J. Am. Chem. Soc 1987, 109 (8), 2546–2547.

(26). Walsdorff C; Saak W; Pohl S A New Preorganized Tridentate Ligand Bearing Three Indolethiolategroups. Preparation of 3:1 Subsite-Differentiated Fe_4S_4 Clusters. J. Chem. Soc. Dalt. Trans 1997, No. 11, 1857–1862.

(27). Ohki Y et al. Synthetic Analogues of $[Fe_4S_4(Cys)_3(His)]$ in Hydrogenases and $[Fe_4S_4(Cys)_4]$ in HiPIP Derived from All-Ferric $[Fe_4S_4\{N(SiMe_3)_2\}_4]$. Proc. Natl. Acad. Sci 2011, 108 (31), 12635–12640. [PubMed: 21768339]

(28). Kanady JS; Tsui EY; Day MW; Agapie T A Synthetic Model of the Mn_3Ca Subsite of the Oxygen-Evolving Complex in Photosystem II. Science 2011, 333 (6043), 733–736. [PubMed: 21817047]

(29). Terada T et al. Tridentate Thiolate Ligands: Application to the Synthesis of the Site-Differentiated [4Fe-4S] Cluster Having a Hydrosulfide Ligand at the Unique Iron Center. Chem. – An Asian J 2012, 7 (5), 920–929.

(30). McSkimming A; Suess DLM Selective Synthesis of Site-Differentiated Fe_4S_4 and Fe_6S_6 Clusters. Inorg. Chem 2018, 57 (23), 14904–14912. [PubMed: 30418746]

(31). Ye M; Thompson NB; Brown AC; Suess DLM A Synthetic Model of Enzymatic $[Fe_4S_4]$–Alkyl Intermediates. J. Am. Chem. Soc 2019, 141 (34), 13330–13335. [PubMed: 31373801]

(32). Brown AC; Suess DLM Controlling Substrate Binding to Fe_4S_4 Clusters through Remote Steric Effects. Inorg. Chem 2019, 58, 5273–5280. [PubMed: 30901206]

(33). McSkimming A; Sridharan A; Thompson NB; Müller P; Suess DLM An $[Fe_4S_4]^{3+}$-Alkyl Cluster Stabilized by an Expanded Scorpionate Ligand. J. Am. Chem. Soc 2020, 142 (33), 14314–14323. [PubMed: 32692919]

(34). Long JR; Williamson AS; Holm RH Dimensional Reduction of $Re_6Se_8Cl_2$: Sheets, Chains, and Discrete Clusters Composed of Chloride-Terminated $[Re_6Q_8]^{2+}$ (Q = S, Se) Cores. Angew. Chemie Int. Ed 1995, 34 (2), 226–229.

(35). Zheng Z; Gray TG; Holm RH Synthesis and Structures of Solvated Monoclusters and Bridged Di-and Triclusters Based on the Cubic Building Block $[Re_6(\mu_3\text{-}Se)_8]^{2+}$. Inorg. Chem 1999, 38 (21), 4888–4895. [PubMed: 11671221]

(36). Champsaur AM et al. Weaving Nanoscale Cloth through Electrostatic Templating. J. Am. Chem. Soc 2017, 139 (34), 11718–11721. [PubMed: 28829133]

(37). Jin S; Adamchuk J; Xiang B; DiSalvo FJ The Dean−Evans Relation in ^{31}P NMR Spectroscopy and Its Application to the Chemistry of Octahedral Tungsten Sulfide Clusters. J. Am. Chem. Soc 2002, 124 (31), 9229–9240. [PubMed: 12149029]

(38). Que L; Bobrik MA; Ibers JA; Holm RH Synthetic Analogs of the Active Sites of Iron-Sulfur Proteins. VII. Ligand Substitution Reactions of the Tetranuclear Clusters $[Fe_4S_4(SR)_4]^{2-}$ and the Structure of $[(CH_3)_4N]_2[Fe_4S_4(SC_6H_5)_4]$. J. Am. Chem. Soc 1974, 96 (13), 4168–4178. [PubMed: 4854592]

(39). Willer MW; Long JR; McLauchlan CC; Holm RH Ligand Substitution Reactions of $[Re_6S_8Br_6]^{4-}$: A Basis Set of Re_6S_8 Clusters for Building Multicluster Assemblies. Inorg. Chem 1998, 37 (2), 328–333.

(40). Reed DA et al. Controlling Ligand Coordination Spheres and Cluster Fusion in Superatoms. J. Am. Chem. Soc 2022, 144 (1), 306–313. [PubMed: 34937334]

(41). Zhou H-C; Holm RH Synthesis and Reactions of Cubane-Type Iron−Sulfur−Phosphine Clusters, Including Soluble Clusters of Nuclearities 8 and 16. Inorg. Chem 2003, 42 (1), 11–21. [PubMed: 12513073]

(42). Zheng Z; Long JR; Holm RH A Basis Set of Re_6Se_8 Cluster Building Blocks and Demonstration of Their Linking Capability: Directed Synthesis of an $Re_{12}Se_{16}$ Dicluster. J. Am. Chem. Soc 1997, 119 (9), 2163–2171.

(43). Harmjanz M; Saak W; Haase D; Pohl S Aryl Isonitrile Binding to $[Fe_4S_4]$ Clusters: Formation of $[Fe_4S_4]^+$ and $[\{Fe_4S_4\}_2]^{2+}$ Cores. Chem. Commun 1997, 0 (10), 951–952.

(44). Champsaur AM et al. Building Diatomic and Triatomic Superatom Molecules. Nano Lett. 2016, 16 (8), 5273–5277. [PubMed: 27410225]

(45). Steigerwald ML et al. Effect of Diverse Ligands on the Course of a Molecules-to-Solids Process and Properties of Its Intermediates. Inorg. Chem 1994, 33 (15), 3389–3395.

(46). Goh C; Segal BM; Huang J; Long JR; Holm RH Polycubane Clusters: Synthesis of $[Fe_4S_4(PR_3)_4]^{1+,0}$ (R = Bu^t, Cy, Pr^i) and $[Fe_4S_4]^0$ Core Aggregation upon Loss of Phosphine. J. Am. Chem. Soc 1996, 118 (47), 11844–11853.

(47). Fuhr O; Dehnen S; Fenske D Chalcogenide Clusters of Copper and Silver from Silylated Chalcogenide Sources Chalcogenide Clusters of Copper and Silver from Silylated Chalcogenide Sources. Chem. Soc. Rev 2013, 42 (4), 1871. [PubMed: 22918377]

(48). Drance MJ et al. Controlled Expansion of a Strong-Field Iron Nitride Cluster: Multi-Site Ligand Substitution as a Strategy for Activating Interstitial Nitride Nucleophilicity. Angew. Chemie Int. Ed 2018, 57 (40), 13057–13061.

(49). Loewen ND; Pattanayak S; Herber R; Fettinger JC; Berben LA Quantification of the Electrostatic Effect on Redox Potential by Positive Charges in a Catalyst Microenvironment. J. Phys. Chem. Lett 2021, 12 (12), 3066–3073. [PubMed: 33750139]

(50). Cammack R Iron—Sulfur Clusters in Enzymes: Themes and Variations. In Advances in inorganic chemistry; Elsevier, 1992; Vol. 38, pp 281–322.

(51). Rees DC; Howard JB The Interface between the Biological and Inorganic Worlds: Iron-Sulfur Metalloclusters. Science 2003, 300 (5621), 929–931. [PubMed: 12738849]

(52). Rouault TA Iron-Sulfur Proteins Hiding in Plain Sight. Nat. Chem. Biol 2015, 11 (7), 442–445. [PubMed: 26083061]

(53). Bista D et al. High-Spin Superatom Stabilized by Dual Subshell Filling. J. Am. Chem. Soc 2022, 144 (11), 5172–5179. [PubMed: 35289175]

(54). Deng L; Holm RH Stabilization of Fully Reduced Iron− Sulfur Clusters by Carbene Ligation: The $[Fe_nS_n]^0$ Oxidation Levels (n = 4, 8). J. Am. Chem. Soc 2008, 130 (30), 9878–9886. [PubMed: 18593124]

(55). Díez-González S; Nolan SP Stereoelectronic Parameters Associated with N-Heterocyclic Carbene (NHC) Ligands: A Quest for Understanding. Coord. Chem. Rev 2007, 251 (5–6), 874–883.

(56). Huang J; Stevens ED; Nolan SP; Petersen JL Olefin Metathesis-Active Ruthenium Complexes Bearing a Nucleophilic Carbene Ligand. J. Am. Chem. Soc 1999, 121 (12), 2674–2678.

(57). Weskamp T; Schattenmann WC; Spiegler M; Herrmann WA A Novel Class of Ruthenium Catalysts for Olefin Metathesis. Angew. Chemie Int. Ed 1998, 37 (18), 2490–2493.

(58). Brown AC; Suess DLM Reversible Formation of Alkyl Radicals at $[Fe_4S_4]$ Clusters and Its Implications for Selectivity in Radical SAM Enzymes. J. Am. Chem. Soc 2020, 142 (33), 14240–14248. [PubMed: 32696642]

(59). Sridharan A; Brown AC; Suess DLM A Terminal Imido Complex of an Iron–Sulfur Cluster. Angew. Chemie Int. Ed 2021, 60 (23), 12802–12806.

(60). Brown AC; Thompson NB; Suess DLM Evidence for Low-Valent Electronic Configurations in Iron-Sulfur Clusters. J. Am. Chem. Soc 2022, 144 (20), 9066–9073. [PubMed: 35575703]

(61). Ye M; Brown AC; Suess DLM Reversible Alkyl-Group Migration between Iron and Sulfur in $[Fe_4S_4]$ Clusters. J. Am. Chem. Soc 2022, 144 (29), 13184–13195. [PubMed: 35830717]

(62). Brown AC; Suess DLM Valence Localization in Alkyne and Alkene Adducts of Synthetic $[Fe_4S_4]^+$ Clusters. Inorg. Chem 2022.

(63). Kim Y; Sridharan A; Suess DLM The Elusive Mononitrosylated $[Fe_4S_4]$ Cluster in Three Redox States. Angew. Chemie Int. Ed 2022, 61 (47), e202213032.

(64). Tan LL; Holm RH; Lee SC Structural Analysis of Cubane-Type Iron Clusters. Polyhedron 2013, 58, 206–217. [PubMed: 24072952]

(65). Guzei IA; Wendt M An Improved Method for the Computation of Ligand Steric Effects Based on Solid Angles. Dalt. Trans 2006, No. 33, 3991–3999.

(66). Falivene L et al. Towards the Online Computer-Aided Design of Catalytic Pockets. Nat. Chem 2019, 11 (10), 872–879. [PubMed: 31477851]

(67). Goddard CA; Long JR; Holm RH Synthesis and Characterization of Four Consecutive Members of the Five-Member $[Fe_6S_8(PEt_3)_6]^{n+}$ (n = 0–4) Cluster Electron Transfer Series. Inorg. Chem 1996, 35 (15), 4347–4354. [PubMed: 11666650]

(68). Huang J; Schanz HJ; Stevens ED; Nolan SP Stereoelectronic Effects Characterizing Nucleophilic Carbene Ligands Bound to the Cp*RuCl (Cp* = η_5-C_5Me_5) Moiety: A Structural and Thermochemical Investigation. Organometallics 1999, 18 (12), 2370–2375.

(69). Nelson DJ; Nolan SP Quantifying and Understanding the Electronic Properties of N-Heterocyclic Carbenes. Chem. Soc. Rev 2013, 42, 6723. [PubMed: 23788114]

(70). Durham JL; Wilson WB; Huh DN; Mcdonald R; Szczepura LF Organometallic Rhenium(III) Chalcogenide Clusters: Coordination of N-Heterocyclic Carbenes. Chem. Commun 2015, 51 (52), 10536–10538.

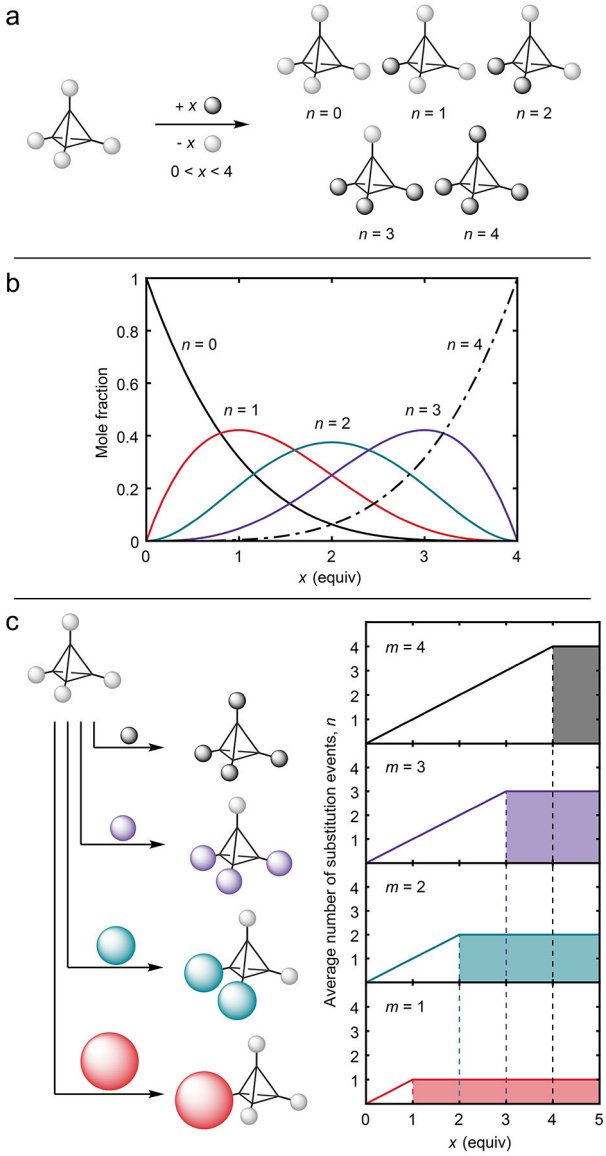

Figure 1.

Challenges in metallocluster site-differentiation illustrated for a tetrahedral cluster. (**a**) Products resulting from unselective substitution of tetrahedral clusters. (**b**) Binomial distribution model of stochastic ligand substitution at a tetrahedral cluster. $n = 0$, 1, 2, 3, and 4 given by the black, red, teal, purple, and dotted traces, respectively (see SI for details about the mathematical model). (**c**) This work. *Left*: limiting the maximal substitution number, m, by tuning the steric properties of the incoming ligand. *Right*: average substitution number of the product distribution as a function of amount added ligand, x. For ligands that dictate $m =$ 4, 3, 2, and 1 (given by the black, purple, teal, and red traces, respectively), precise patterns of site-differentiation are obtained for $x \geq m$.

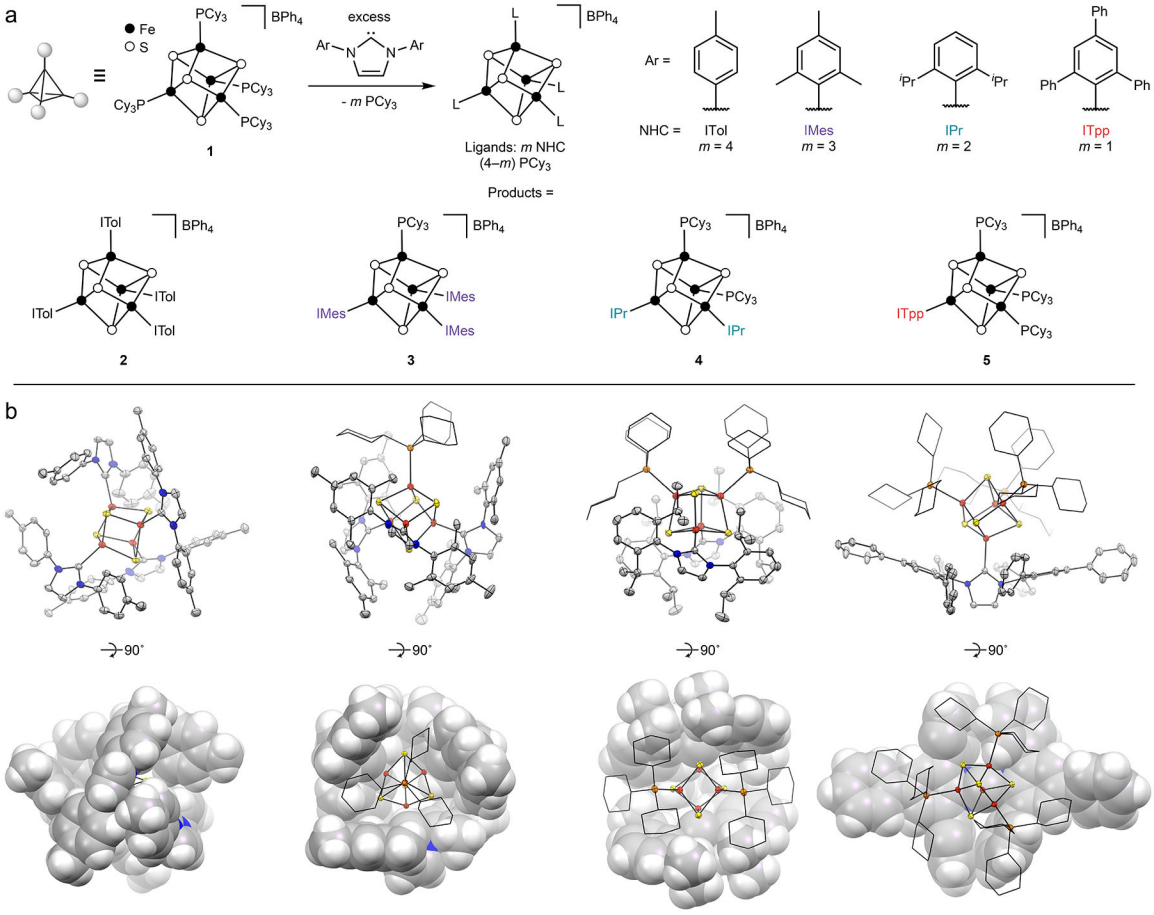

Figure 2.

Site differentiation of $[Fe_4S_4]^+$ clusters using remote steric effects. (**a**) Synthesis; ligands color-coded as in Fig. 1b. (**b**) Thermal ellipsoid plots (50%; top) and corresponding space-filling illustrations (rotated 90°; bottom) of **2**, **3**, **4**, and **5** (left to right). Hydrogen atoms, counter ions, solvent molecules, and thermal ellipsoids of PCy_3 ligands omitted for clarity. Color scheme: Fe (red-orange), S (yellow), P (orange), N (blue), C (grey).

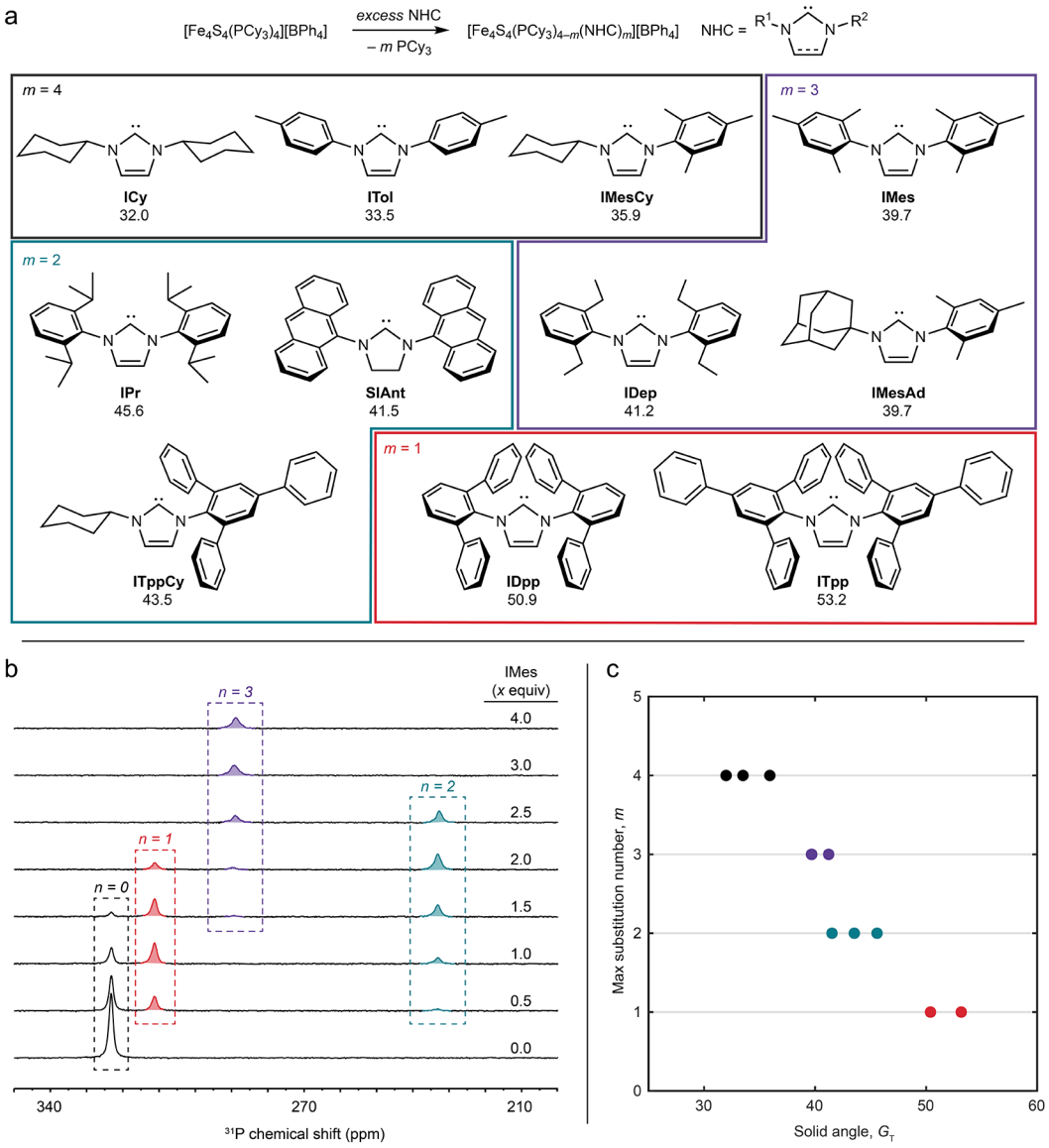

Figure 3.

Expanding the scope of site-differentiation to develop a predictable model for determining the maximum number of substitution events, *m*. (**a**) Chart of NHCs and their theoretical solid angles (G_T) organized according to their observed *m* values. (**b**) ^{31}P NMR traces of the IMes titration reaction. The peaks are assigned as the number of bound IMes ligands, *n*. (**c**) Plot of maximal substitution number, *m*, against computed solid angle, G_T. Note that the points for IMes and IMesAd obscure one another.

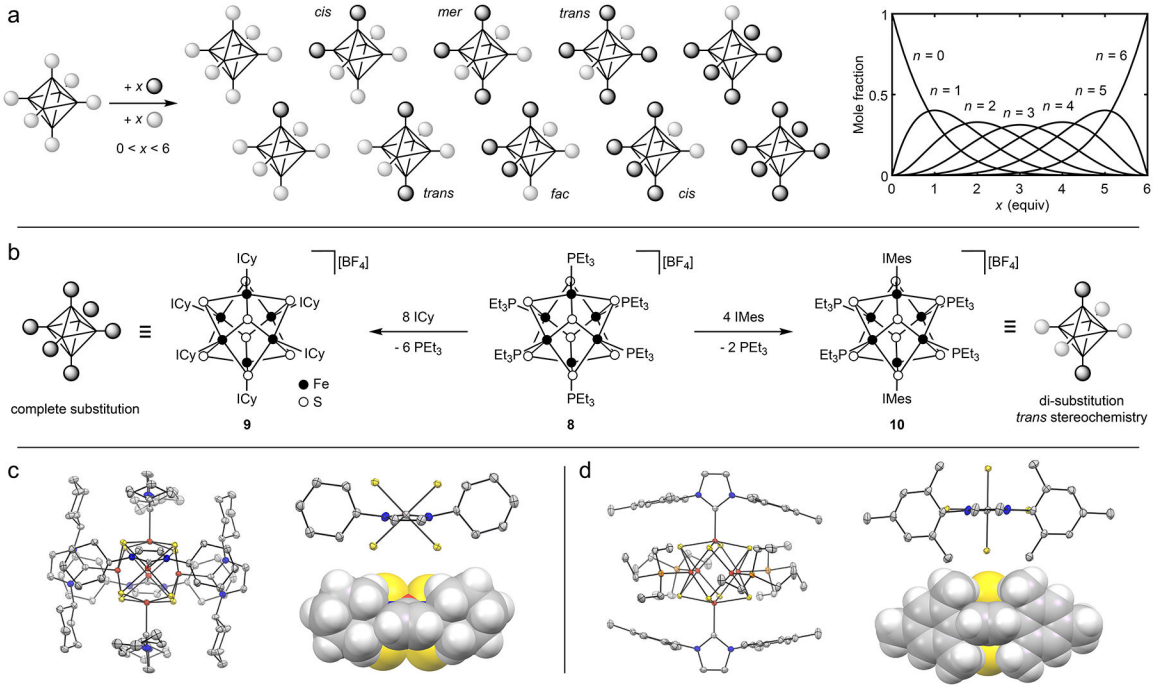

Figure 4.

Stereoselective site-differentiation of $[Fe_6S_8]^+$ clusters. (**a**) Expected product distribution resulting from unselective substitution reactions with octahedral clusters. (**b**) Synthesis of **9** and **10**. (**c-d**) Thermal ellipsoid plots (50%) and space-filling illustration of **9** and **10** as well as an NHC-bound Fe site of each, illustrating the observed ∠SFeCN dihedral angles. Hydrogen atoms, counter ions, solvent molecules, and thermal ellipsoids of PEt_3 ligands omitted for clarity. Color scheme as in Fig. 2b.